

Numerical modeling of upper-room UV germicidal irradiation — Validation and performance comparison under various airflow regimes in a generic enclosure

Claudio Alanis Ruiz^{1*}, Marcel Loomans¹, and Twan van Hooff¹

¹Building Physics and Services, Department of the Built Environment, Eindhoven University of Technology, Netherlands

Abstract. Given the critical importance of containing the spread of infectious airborne pathogens in indoor environments, ultraviolet germicidal irradiation (UVGI) has become increasingly adopted as a non-intrusive technology for controlling microbiologic infections in these settings. However, modeling the disinfection process of UVGI in indoor environments poses challenges because it involves multiple complex physical processes, which are additionally transient in nature. Computational fluid dynamics (CFD) simulations are frequently used to evaluate UVGI performance. Nevertheless, the modeling of such intricate systems is not straightforward and can often be computationally expensive. Here we demonstrate a relatively simple and computationally inexpensive approach using an Eulerian-Eulerian model in CFD to simulate airborne biopollutant transport and UVGI disinfection in a generic enclosure, representing a room. This approach incorporates volumetric biopollutant sinks based on first-order kinetics to approximate the decay of an airborne biopollutant under a UV irradiation field. Subsequently, we validate this numerical approach using recent experimental data from the literature. Finally, we discuss the transient behavior and performance of UVGI disinfection under various airflow regimes relevant to indoor building applications. Specifically, we explore the effects of air mixing, in order to support the biopollutant dispersion, ventilation supply, and the influence of a biopollutant source. The results underscore the significance of air mixing in enhancing the performance of UVGI disinfection under transient and non-equilibrium system conditions.

1 Introduction

In recent years, infectious airborne pathogens have placed significant strain on economies and healthcare systems worldwide. These pathogens have a greater potential to spread in indoor environments due to factors such as ventilation and occupancy conditions, leading to higher pathogen concentrations, and the fact that people spend extended periods indoors.

One technology employed for controlling microbiologic infections in indoor environments is ultraviolet germicidal irradiation (UVGI). This technology utilizes short-wavelength ultraviolet radiation to impede the reproduction ability of airborne microorganisms that come in contact with its emitted radiation field. However, modeling the disinfection process of UVGI in indoor environments presents challenges because it involves multiple complex physical processes, including fluid flow, energy and mass transfer, and is inherently related to transient phenomena. Advective transport depends on momentum and thermal buoyancy interactions, mixing arises from turbulent flow patterns, and molecular diffusion is driven by concentration gradients. Moreover, UV light radiation influences the airborne pathogen concentration field. Since on-site measurements are often not possible and very complex, computational fluid dynamics (CFD)

simulations are the preferred method for assessing the UVGI performance for different configurations. Nevertheless, the modeling of such intricate systems is not straightforward and can often be computationally expensive. Detailed approaches, such as those where a variable, non-uniform irradiation field is explicitly simulated, have been proposed [1-3]. These approaches involve coupling CFD with ray tracing techniques in order to simultaneously solve for fluid flow and radiation (light) transport in the indoor space where the UVGI is active. Ray tracing allows for an accurate determination of the distribution of UV light in a space as it models the emission of multi-directional 3D light sources, as well as the reflection and absorption of light on the surfaces of the computational domain. Other, simpler approaches include steady-state tracer gas [4, 5], particle-tracking (Lagrangian-based) [6-8], and steady-state Eulerian methods [8-10].

In this contribution, we demonstrate a computationally efficient approach using CFD to model UVGI within a generic enclosure, representing a room. This approach involves the integration of a straightforward analytical model into CFD to simulate airborne biopollutant inactivation by UVGI. This approach employs a fairly computationally inexpensive transient Eulerian-Eulerian transport model to simulate the dispersion of the biopollutant, and it incorporates

* Corresponding author: c.a.alanis.ruiz@tue.nl

volumetric biopollutant sinks based on first-order kinetics to approximate the decay of biopollutant concentration under a relatively uniform UV irradiation field. Subsequently, we validate this numerical approach using recent experimental data from the literature. Finally, we discuss the transient behavior and performance of UVGI disinfection under various airflow regimes relevant to indoor building applications. Specifically, we explore the effects of additional air mixing, in order to support the biopollutant dispersion, ventilation supply, and the presence of a biopollutant source.

2 Methods

2.1 UVGI model and CFD implementation

2.1.1 Analytical UVGI model

First-order kinetics are employed to approximate the transient decay of a biopollutant within a differential control volume subjected to the action of a UVGI device. With this modeling approach, the temporal evolution of biopollutant concentration takes the following form:

$$\frac{dc}{dt} = -kc \quad (1)$$

where c is the biopollutant concentration, t the time, and k the decay rate. Note that this equation has been widely used in chemistry applications to model reactant concentrations and radioactive decay/degradation processes. Here, the total decay rate of the biopollutant accounts for the natural degradation of the biopollutant k_{ND} and the inactivation caused by UV irradiation k_{UV} , thus:

$$k = k_{ND} + k_{UV} \quad (2)$$

In the case of UV light exposure, the decay factor k_{UV} can be expressed as a function of the susceptibility of the biopollutant Z and the UV irradiation (or fluence) rate I [11, 12]:

$$k_{UV}[s^{-1}] = Z \left[\frac{m^2}{J} \right] * I \left[\frac{W}{m^2} \right] \quad (3)$$

When applying this model to an operational indoor environment, it is possible to partition the room volume into distinct zones that experience varying degrees of UVGI exposure. Typically, the upper zones receive direct UVGI, while the lower zones, where occupants are situated, receive less irradiation, consequently requiring an adjustment in parameter k_{UV} in each zone. Additionally, there can be punctual or distributed sources of airborne biopollution, such as those emitted by infected individuals. In order to account for these aspects, a contaminant source term S is introduced into **Eq. (1)**, resulting in the following formulation, which is applied to each zone in the room:

$$\frac{dc}{dt} = S - kc \quad (4)$$

The source term S for a given zone can then be computed as:

$$S = S_{bp} + \frac{\dot{m}_{bp}}{V} = S_{bp} + \frac{1}{V} \int x_{bp} \rho (\vec{v} \cdot \vec{n}) dA \quad (5)$$

where S_{bp} is the biopollutant source in that zone, if any, \dot{m}_{bp} is the mass flux of the biopollutant from/to adjacent zones, x_{bp} is the mass fraction of the biopollutant, ρ is the density of the air mixture, \vec{v} the velocity vector, V the volume of the given room zone, A the area of an imaginary surface that divides the zones of the room, and \vec{n} the outward normal vector of this surface.

The general decay patterns of the biopollutant within a control volume under UVGI are depicted in **Figure 1**, using the analytical solution **Eq. (6)** derived from the ordinary differential equation presented above (**Eq. 4**). Various system parameters are explored to illustrate their influence on the decay behavior.

$$c(t) = \frac{S}{k} + B e^{(-kt)} \quad (6)$$

where the integration constant is $B = c_0 - S/k$; with c_0 being the initial biopollutant concentration.

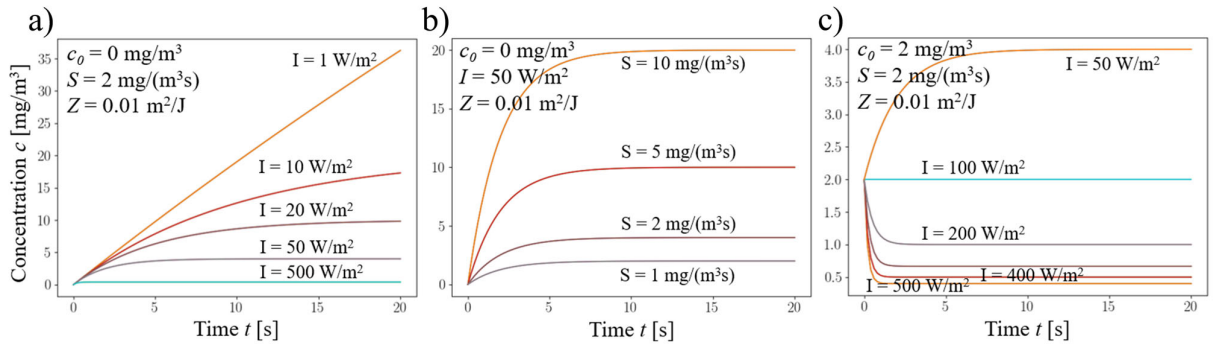


Fig. 1. Evolution of biopollutant concentration with time in a differential control volume under UVGI subjected to various system parameters: a) UV irradiation rate variations, b) biopollutant source term variations, and c) UV irradiation rate variations with a higher initial biopollutant concentration. Note that k_{ND} is neglected in these plots.

2.1.2 CFD implementation

The computational domain is initially partitioned into distinct zones depending on their irradiation level and sources of pollution. Eq. (4) and (5) are subsequently applied as volumetric sources or sinks for the biopollutant in each volumetric zone. Note that in CFD, the integral (second) term of Eq. (5) is typically calculated automatically when coupling and enabling an Eulerian species transport model.

2.2 Validation

2.2.1 Experimental setup

Disinfection experiments of an upper-room UVGI system in a full-scale chamber were reported recently in literature [13]. The configuration of these experiments is indicated in Figure 2. It consisted of a chamber with dimensions (L × W × H) 2.25 × 2.3 × 2.3 m³ where an UVGI device (a far-UVC 222 nm light source emitted by a 15 W Krypton-chloride lamp; Ushio Care 222) was installed in the upper zone of the chamber at 2 m from the floor level. The distribution of UV irradiation in the chamber was measured at uniformly distributed points and reported for four different planes at heights of 0.5, 1, 1.5, and 2 m from the floor level.

Bioaerosol was injected and its concentration was sampled through a small opening at a height of 1.5 m (see Figure 2). The bioaerosol, consisting of a bacterial suspension, was tested for the decay of four distinct bacterial colonies in the experiments; however, the CFD validation presented here specifically focuses on the common *Escherichia coli* (*E.coli*).

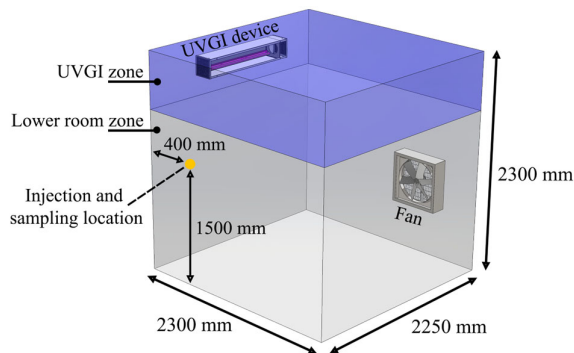


Fig. 2. Graphical representation of the experimental setup, as described in [13].

The preparation procedure before activating the UVGI device and subsequent sampling of airborne bacterial concentrations involved injecting the aerosolized bacterial suspension into the chamber. The bioaerosol was then mixed with air in the chamber using a fan. The fan was turned off during the operation of the UVGI device and the sampling of airborne bacterial concentrations. The bacterial concentration sampling occurred every 2 minutes for a total duration of 10 minutes, thus resulting in 6 data points per experiment. The length of each sampling event lasted 25 seconds at a flow rate of 28.3 L/min.

2.2.2 CFD simulations

The experimental setup is replicated in a 3D computational domain for CFD simulations. The dimensions of the domain correspond to those shown in Figure 2. A uniform hexahedral grid with 7,500 cells was created, which is displayed in Figure 3. The low cell count needed for this specific simulation is due to the absence of air movement reported during the concentration sampling phase of the experiments. This simplification reduces the complexity of the physics to be numerically resolved in the validation study.

An advection-diffusion equation is solved to account for the biopollutant transport and decay. Two species are introduced into an air mixture that comprises the system: (1) clean air and (2) a bioaerosol suspension. Both species are assumed to have the same physical properties in terms of density, viscosity and mass diffusivity. This assumption is made because the aerosolized biopollutant suspension injected into the chamber during the experiments is sufficiently diluted, minimizing its influence on these properties.

The UVGI model is implemented as detailed in Section 2.1.2. For this, the computational domain is vertically divided into 5 zones, each corresponding to different heights aligned with the planes where UV irradiation is measured in the experiments. The lowest zone is assumed to receive no UV irradiation. Eq. (4) is then introduced as a volumetric bioaerosol source (or sink) in each zone, taking the mean value of the measured UV irradiation at 100% power output of the UVGI device in the respective plane as I in Eq. (3) (see Table 1). The susceptibility to UV exposure and the natural decay rate of *E.coli* are constants as reported in the experiments: $Z = 0.974 \text{ m}^2/\text{J}$ and $k_{ND} = 0.0026 \text{ s}^{-1}$.

Table 1. Mean UV irradiation I for each zone of the partitioned computational domain.

Volumetric cell zone	Height [m]	Mean UV irradiation I [$\mu\text{W}/\text{cm}^2$]
Zone 1	0 – 0.25	0
Zone 2	0.25 – 0.75	0.16
Zone 3	0.75 – 1.25	0.31
Zone 4	1.25 – 1.75	0.56
Zone 5	1.75 – 2.3	1.88

Concerning the boundary conditions, all surfaces of the computational domain are treated as smooth walls with zero diffusive flux. In terms of the initial condition for concentration in the CFD simulations, a starting bioaerosol suspension concentration of 100% mass fraction is used.

Throughout the experiments, air temperature and humidity parameters in the chamber were kept nearly constant, therefore these parameters and their

corresponding transport equations are not considered in the CFD simulations.

The system is solved numerically in CFD by means of the 3D unsteady Reynolds-averaged Navier-Stokes (URANS) method using ANSYS Fluent 2023. Given the absence of air movement in the specific case of this validation study, only the species diffusion equation is solved. Second-order schemes are applied for the discretization of the spatial and temporal terms in the equation.

The numerical solution spans a duration of 10 minutes with a constant time-step $\Delta t = 1$ s. Convergence is considered achieved when the scaled residuals of the variable reaches at least 10^{-4} for each time step.

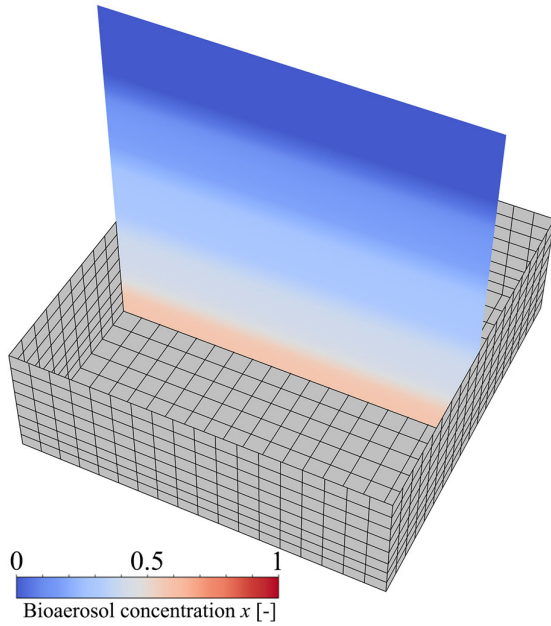


Fig. 3. Visualization of part of the computational domain and grid used in the CFD validation study. The superimposed vertical midplane contour displays the distribution of bioaerosol concentration (mass fraction) at $t = 200$ s.

2.2.3 Comparison of numerical and experimental results

The experimental data from literature is compared to the numerical simulation results in terms of the normalized *E.coli* suspension concentration $\ln(c_i/c_0)$, which decays over time due to the UVGI activity. The experiments were repeated four times, hence four markers representing discrete concentration measurements are shown in **Figure 4**.

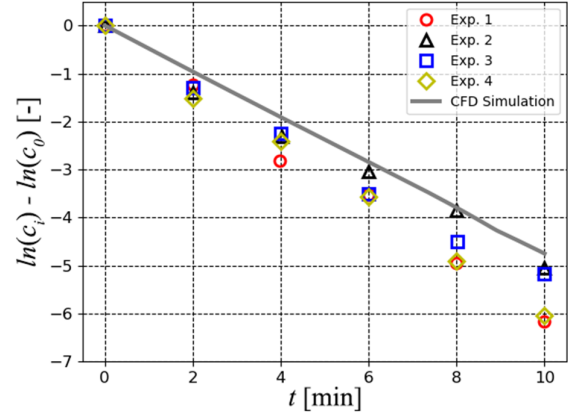


Fig. 4. Comparison between the present CFD simulation and experimental results from [13] illustrating the decay of *E.coli* in the chamber under UVGI at 100% power output.

The numerical simulations using the proposed approach follow the expected behavior and exhibit a good agreement with the experiments, especially with measurement set #2, although the overall decay of bioaerosol is underestimated in the simulations. It should be noted, however, that the experimental data displays a progressively higher variance over time, suggesting that simulations results fall within the confidence range of the experiments, considering uncertainties.

3 Performance of UVGI

With the validated UVGI model, the transient behavior and performance of the UVGI system in increasingly complex and more realistic indoor airflow scenarios is examined. These scenarios encompass diverse levels of air mixing, ventilation supply, and the introduction of a biopollutant source. The following scenarios are analyzed:

- Ventilation + air mixing (no UVGI)
- UVGI + reduced air mixing
- UVGI + air mixing
- UVGI + enhanced air mixing
- UVGI + reduced air mixing + pollutant source
- UVGI + air mixing + pollutant source
- UVGI + enhanced air mixing + pollutant source
- UVGI + ventilation + air mixing + pollutant source

For the CFD simulation of these additional scenarios, the dimensions of the computational domain remain unchanged. However, an internal fan is activated within the domain, aligning with the location of the fan in the experiments. Three levels of air mixing are explored, wherein the air velocity magnitude $|V|$, considering axial and tangential velocity components originating from the fan, is adjusted as follows: 0.47 m/s for reduced air mixing, 0.97 m/s for air mixing, and 1.88 m/s for enhanced air mixing. Additionally, a volumetric pollution source encompassing the bottom zone (#1) is introduced. The biopollutant source is constant and represents $\frac{1}{2}$ of the biopollutant inactivation potential by UV irradiation in the top UVGI zone, resulting in $S_{bp} =$

0.0128 kg/(m³s). Furthermore, the domain includes a ventilation inlet situated behind the fan and a zero static gauge pressure outlet on the top wall (ceiling) as boundary conditions. The ventilation rate is specified to deliver 6 air changes per hour (ACH).

The UVGI model implementation remains unchanged and it uses the same parameters described before. All the simulations in this section are initialized with the fan in operation and with a bioaerosol suspension concentration of 100% mass fraction.

The computational grid is adjusted to account for the more complex fluid flow physics. Consequently, the grid here consists of 107,100 structured hexahedral cells with particular refinement in areas anticipating larger velocity gradients due to the presence of the interior fan, ventilation inlet and outlet. The updated computational domain and grid are visualized in **Figure 5**.

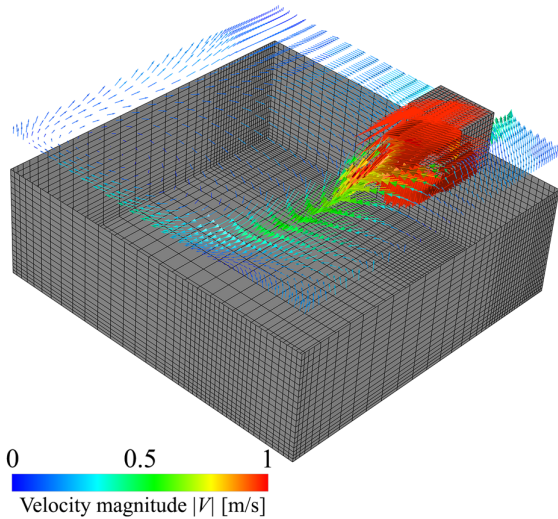


Fig. 5. Updated computational domain and grid with velocity vectors colored by magnitude in a horizontal plane at the midheight of the interior fan.

The computational configuration of these additional scenarios is similar to the one presented for the validation study in **Section 2.2.2**. However, here the URANS equations are solved in full including momentum and continuity, and bioaerosol advective-diffusive transport based on an Eulerian-Eulerian approach. Closure to the equations is provided by means

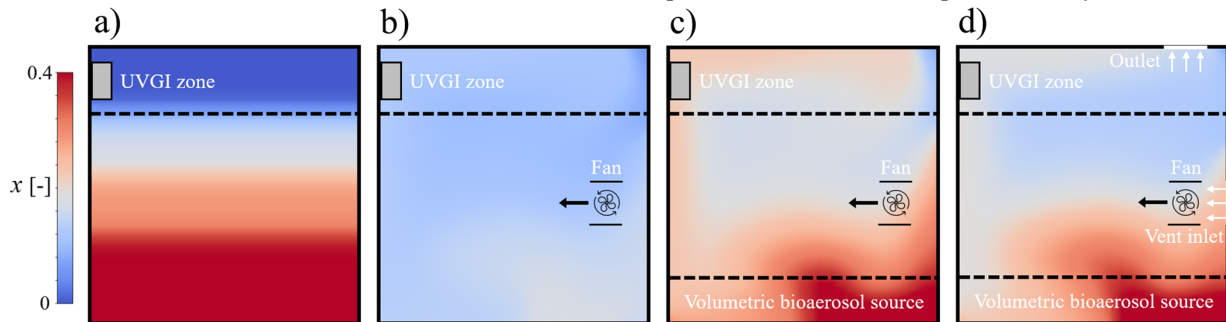


Fig. 6. Instantaneous bioaerosol concentration distributions in the vertical midplane of the chamber at $t = 220$ s, representing approximately one-third of the time to reach equilibrium: a) validation scenario (no air mixing, no pollution sources and no ventilation), b) air mixing scenario, c) air mixing with pollutant source scenario, and d) air mixing with pollutant source and ventilation scenario.

of the realizable k - ϵ turbulence model. Scalable wall functions are employed. Similarly to the validation case, second-order schemes are applied for the transient formulation and the spatial discretization of all flow variables. Pressure-velocity coupling is achieved through the Pressure Implicit with Slip Operator (PISO) algorithm.

The time-step for these simulations is set to $\Delta t = 0.1$ s to comply with the Courant–Friedrichs–Lewy condition. The numerical solutions cover a duration of 600 seconds of real flow time, representing approximately the time it takes for the system to reach a state of equilibrium. The same convergence criteria as employed in the validation study are used, requiring that the scaled residuals of all flow variables reach at least 10^{-4} in each time step.

For the presentation of results, volume-averaged bioaerosol concentrations in the chamber are reported over time for each scenario. Instantaneous bioaerosol concentration data is also displayed for selected scenarios. Results are shown in **Figures 6** and **7**.

3.1 Influence of air mixing

In comparison to the case with no air mixing, it is evident that air mixing significantly improves UVGI performance before reaching the state of equilibrium. Bioaerosol concentrations decrease up to 18% faster when air mixing is applied. This is attributed to air mixing facilitating the degradation of biopollutants from the lower zones of the chamber by transporting them to the upper zones where the UVGI device is more active. Without air movement, the pollutants in the lower zones would be exposed to lower UV irradiation levels, leading to a slower decay. Naturally, after reaching equilibrium and in the absence of a zonal pollutant source, mean concentrations in the chamber between air mixing and no air mixing scenarios are identical, in consistency with the mass conservation principle.

An interesting observation is the influence of air mixing levels. Simulations conducted both with and without the pollutant source reveal that a higher level of air mixing corresponds to a higher pollutant removal performance in the chamber, as shown in **Figure 7**. However, the rate of change between reduced-to-intermediate and intermediate-to-enhanced air mixing scenarios suggests a limit on the achievable UVGI performance based on this parameter. Beyond a certain

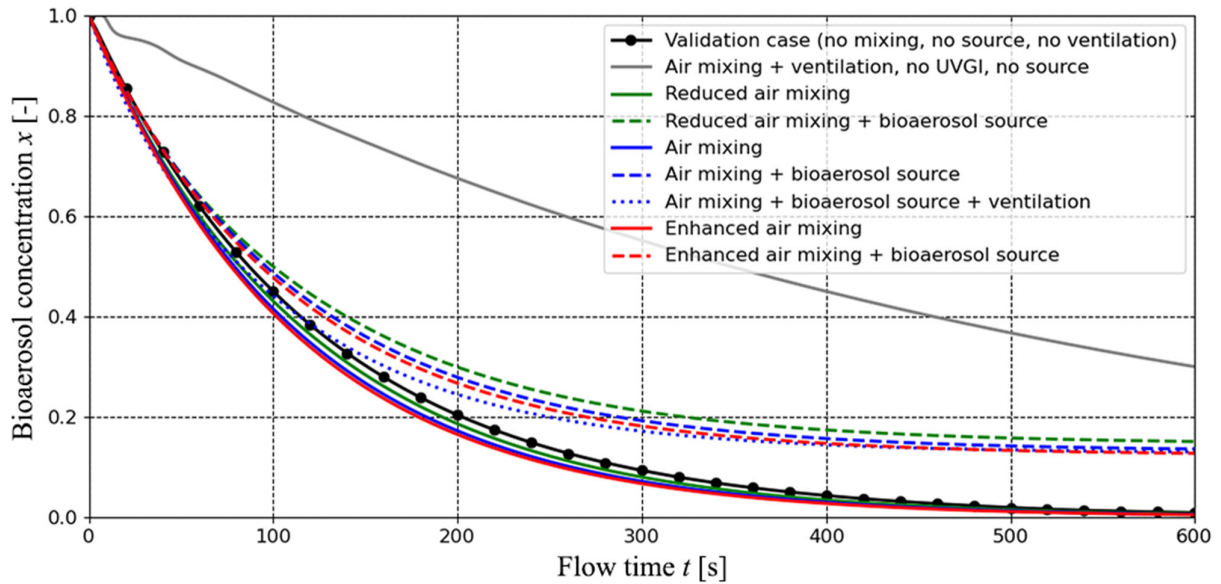


Fig. 7. Temporal evolution of volume-averaged *E. coli* bioaerosol concentration in the chamber under UVGI for the various simulated scenarios.

level of air mixing, additional air movement hardly leads to improvements in pollutant removal performance via UVGI.

Local effects on concentration distribution, not reflected in volume-averaged data, are observed. Some areas near the left-hand side wall and ceiling exhibit higher biopollutant concentrations with increased air mixing—a contrast to the impact on volume-averaged concentration, which shows the opposite trend. These local effects are caused by the fan directing air from lower zones that have higher pollutant concentrations because of the reduced UV irradiation and the presence of a pollutant source. Nevertheless, the mentioned local effects are limited in space and time, and thus they have less overall significance.

3.2 Influence of pollutant source

The introduction of a pollutant source has a straightforward impact. In terms of temporal evolution, the concentration consistently exhibits a slower decay and settles at a higher concentration level once equilibrium is reached. Regarding the pollutant distribution (**Figure 6c,d**), concentrations are notably higher near the source location. Additionally, relatively high pollutant concentrations are observed near the left-hand side wall and ceiling as the flow attaches to these surfaces in a circular motion induced by the momentum injected by the fan.

3.3 Influence of ventilation

The introduction of ventilation, in combination with air mixing and UVGI, results in a visible decrease in concentrations throughout, especially in the initial simulation period, thereby to some extent counteracting the impact of the pollutant source. However, despite 6 ACH being a common ventilation rate in practice, the global impact is somewhat limited under the simulated

parameters of the system. For this specific case, the ventilation exhaust is positioned in the top zone to prevent short-circuiting from the ventilation inlet, but this is also the location where the UVGI is most active.

A scenario with ventilation alone (without UVGI) is compared to scenarios incorporating UVGI in **Figure 7**. In the former, there is a nearly linear decrease in biopollutant concentration, albeit at a slower pace than in scenarios with UVGI. In practice, the relative performance of biopollutant removal via ventilation against UVGI would also depend on additional parameters, such as air distribution configuration, the position of the ventilation exhaust, ventilation supply rate, buoyancy sources, and UV irradiation, which are held constant in this study. Nevertheless, UVGI appears to be a more efficient and practical approach for biopollutant removal compared to increased ventilation.

4 Discussion

Discrepancies between experimental and simulation results may arise from: (1) zonal averaging of UV irradiation instead of using a detailed distribution of the UVGI field (e.g., [1-3]), (2) potential air movement effects not documented in the experiments, such as air extraction during sampling or lingering air mixing after the fan is turned off, and (3) other simplifications in the physics and properties of the gas mixture, such as not accounting for density differences in the mixture and for possible aerosol deposition on walls. In spite of that, the UVGI modeling approach demonstrated here is computationally inexpensive (in relative terms), easy to implement using CFD and yields acceptable results, making it a practical and cost-effective method for approximating the effect of an UVGI system as part of a mitigation solution for biopollutants. Furthermore, the transient mathematical model employed for UVGI in this study offers the potential to integrate real-time data concerning occupancy or indicators of air quality, which

can be linked to the sources of biopollution in a room. This integration would enable the transient control of UV irradiation, aiming to optimize the performance of the UVGI device. However, since CFD does not support real-time computations of the flow field, such an approach would require the utilization of low-order numerical models or machine learning to achieve faster, nearly real-time flow predictions and optimization of UVGI control.

The scenarios presented in the last part of this investigation are simplified, limited in number, and designed for a generic purpose. They are not intended to depict a specific UVGI system or indoor environment. Instead, their aim is to illustrate the general behavior of UVGI and demonstrate its performance under influential system parameters. In addition to the generic enclosure scenario presented here, limitations of the UVGI modeling approach in real room situations may stem from the complexity of such scenarios. These complexities can include human interactions, dynamic and non-uniform distributions of heat, biopollution, and radiation sources, and various ventilation and air distribution configurations. While the fundamental mathematical formulation for the UVGI system remains valid, addressing these aspects may require coupling the mathematical model with more advanced and computationally intensive CFD methods. Therefore, a more realistic representation of a UVGI system in more complex indoor environments, including irregular room geometries and some of the factors mentioned above, could prove beneficial and expand on the information provided here.

Finally, this study, consistent with the experimental data from the literature, employs *E.coli* as a surrogate to represent an airborne biopollutant. It is important to note that the susceptibility factor (Z) of *E.coli* to UV irradiation is relatively high. This factor should be taken into account when interpreting the results presented in **Section 3**. The decay rate of the biopollutant under the UV irradiation provided by the UVGI device may vary depending on the specific airborne microorganism being considered.

5 Conclusions

In this paper a relatively simple and efficient approach for modeling UVGI using CFD is demonstrated and validated using recent experimental data from literature. Using this model, the performance of a generic upper-room UVGI system is evaluated under parameters relevant for indoor building applications.

Validation results show that while the UVGI model implemented in CFD slightly underpredicts biopollutant concentration decay compared to experimental data, the numerical predictions are still in fairly good agreement and are considered reasonably accurate, making the numerical approach computationally cost-effective.

Concerning UVGI performance, air mixing proves crucial for optimal upper-room UVGI efficiency. An appropriately mixed environment supports faster biopollutant inactivation, especially under transient and non-equilibrium conditions. Ventilation is beneficial for

reducing room biopollutant concentrations; however, the simulation results under the set of parameters used here indicate that UVGI can be potentially more effective for biopollutant inactivation. Therefore, an optimal strategy should involve a combination of UVGI with adequate ventilation and air mixing.

Acknowledgement

The research presented is part of the collaboration project CLAIRE (LSHM22032), co-funded by the PPP Allowance made available by Health~Holland, Top Sector Life Sciences & Health, to stimulate public-private partnerships (<https://www.health-holland.com/>). We would like to thank Health~Holland for this, as well as the partners involved in the project.

Nomenclature

A	=	area of surface [m ²]
B	=	integration constant [-]
c	=	biopollutant concentration [mg/m ³] or [-]
c_0	=	initial concentration [mg/m ³] or [-]
I	=	UV irradiation or fluence rate [W/m ²]
k	=	total decay rate [s ⁻¹]
k_{ND}	=	natural decay rate of the biopollutant [s ⁻¹]
k_{UV}	=	decay rate of the biopollutant due to UV exposure [s ⁻¹]
\dot{m}_{bp}	=	mass flux of biopollutant [kg/m ² s]
\vec{n}	=	outward normal vector of surface [-]
S	=	biopollutant source [mg/m ³ s] or [s ⁻¹]
S_{bp}	=	biopollutant source in a particular zone [mg/m ³ s] or [s ⁻¹]
t	=	time [s]
\vec{v}	=	velocity vector [m/s]
V	=	volume of the zone [m ³]
$ V $	=	velocity magnitude [m/s]
x_{bp}	=	mass fraction of biopollutant [-]
Z	=	susceptibility of the biopollutant to UV irradiation [m ² /J]
ρ	=	density of the air mixture [kg/m ³]

References

1. M. Hou, J. Kim, J. Pantelic and D. Aviv, "Integration of raytracing and CFD simulation to assess the impact of UVGI technology on the control of aerosol transmission in an occupied room," in Proceedings of IBPSA Building Simulation 2021, Bruges, Belgium, (2021)
2. M. Hou, J. Pantelic and D. Aviv, "Spatial analysis of the impact of UVGI technology in occupied rooms using ray-tracing simulation," *Indoor Air*, **31**:5, pp. 1625-1638, (2021)

3. H. Luo and L. Zhong, “*Numerical Analysis of Effects of Ventilation Conditions on an In-duct UVGI System for Infection Control*,” in Proceedings of Conference on Building Energy and Environment (COBEE) 2022, Montreal, Canada, (2022)
4. C.J. Noakes, L.A. Fletcher, P.A. Sleight, W.B. Booth, B. Beato-Arribas and N. Tomlinson, “*Comparison of Tracer Techniques for Evaluating the Behaviour of Bioaerosols in Hospital Isolation Rooms*,” in Proceedings of Healthy Buildings 2009, Syracuse, USA, (2009)
5. S. Park, R. Mistrick and D. Rim, “*Performance of upper-room ultraviolet germicidal irradiation (UVGI) system in learning environments: Effects of ventilation rate, UV fluence rate, and UV radiating volume*,” *Sustainable Cities and Society*, **85**, Art. 104048, (2022)
6. H. Motamedi, M. Shirzadi, Y. Tominaga and P.A. Mirzaei, “*CFD modeling of airborne pathogen transmission of COVID-19 in confined spaces under different ventilation strategies*,” *Sustainable Cities and Society*, **76**, Art. 103397, (2022)
7. P. Xu, N. Fisher and S. Miller, “*Using Computational Fluid Dynamics Modeling to Evaluate the Design of Hospital Ultraviolet Germicidal Irradiation Systems for Inactivating Airborne Mycobacteria*,” *Photochemistry and Photobiology*, **89**:4, pp. 792-798, (2013)
8. G. Pichurov, J. Srebric, S. Zhu, R.L. Vincent, P.W. Brickner and S.N. Rudnick, “*A validated numerical investigation of the ceiling fan's role in the upper-room UVGI efficacy*,” *Building and Environment*, **86**, pp. 109-119 (2015)
9. C.A. Gilkeson and C. Noakes, “*Application of CFD Simulation to Predicting Upper-Room UVGI Effectiveness*,” *Photochemistry and Photobiology*, **89**, pp. 799-810, (2013)
10. M. Kannan, “*CFD optimization of return air ratio and use of upper room UVGI in combined HVAC and heat recovery system*,” *Case Studies in Thermal Engineering*, **15**, Art. 100535, (2019)
11. W. Kowalski, W. Bahnfleth, D. Witham, B. Severing and T. Whittam, “*Mathematical Modeling of Ultraviolet Germicidal Irradiation for Air Disinfection*,” *Quantitative Microbiology*, pp. 2: 249-270, (2000)
12. McDevitt, Rudnick and Radonovich, “*Aerosol Susceptibility of Influenza Virus to UV-C Light*,” *Applied and Environmental Microbiology*, **78**:6, (2012)
13. M. Wang, H. Zhang, C. Chan, P. Lee and A. Lai, “*Experimental study of the disinfection performance of a 222-nm Far-UVC upper-room system on airborne microorganisms in a full-scale chamber*,” *Building and Environment*, **236**: Art. 110260, (2023)